Design, Synthesis, and Photophysical Characterization of Biocompatible Thermally Activated Delayed Fluorescent Carbazole-Coumarins for Sensing Applications.

Andrea Cocco,[a][b] Sara Paniziutti,[a][b] Chiara Olla,[c] Riccardo Corpino,[c] Carlo Maria Carbonaro,[c]* Pier Carlo Ricci,[c] Nicola Melis,[d] Paola Caria,[e] Giuseppina Sanna,[e] Eli Zysman-Colman,[b]* and Francesco Secci[a]*

[a]   *Prof. Francesco Secci, Dr. Andrea Cocco, Dr. Sara Paniziutti, Dept. of Chemical and Geological Sciences, Università degli Studi di Cagliari, 09042 Monserrato (Cagliari) ITALY e-mail: fsecci@unica.it*

[b]   *Prof. Eli Zysman Colman, Dr. Andrea Cocco, Dr. Sara Paniziutti, Organic Semiconductor Centre, EaStCHEM School of Chemistry, University of St Andrews, Fife KY16 9ST, UK e-mail: eli.zysman-colman@st-andrews.ac.uk*

[c]   *Prof. Carlo Maria Carbonaro, Prof. Pier Carlo Ricci, Dr. Riccardo Corpino, Dr. Chiara Olla, Department of Physics, Università degli Studi di Cagliari, 09042 Monserrato (Cagliari) ITALY, e-mail: cm.carbonaro@dsf.unica.it*

[d]   *Dr. Nicola Melis, Department of Mechanical, Chemical and Materials Engineering Università degli Studi di Cagliari, 09123, via Marengo 2, Cagliari, ITALY*

[e]   *Prof. P. Caria, Dr. G. Sanna, Department of Biomedical Sciences, Università degli Studi di Cagliari, 09042 Monserrato (Cagliari) ITALY*

Abstract

A series of fluorescent carbazole-coumarins exhibiting good photoluminescence quantum yields and thermally activated delayed fluorescence (TADF) properties have been designed and synthetized using computer-aided density functional theory calculations. The TADF characteristics of the carbazole-coumarins were systematically explored both in solution and in the solid state, utilizing poly(methyl methacrylate) (PMMA) as a matrix. The study revealed that the introduction of carbazole units onto the coumarin benzene ring led to compounds with thermally induced reverse intersystem crossing and delayed fluorescence. The study further demonstrated the potential utility of these compounds in practical applications by incorporating them into a Cmr-PMMA-based sensor for molecular oxygen detection. The resulting sensor exhibited promising performance, highlighting the adaptability and efficacy of the synthesized TADF-carbazole-coumarin compounds for reversible molecular oxygen sensing.

Keywords: Coumarins, TADF-compounds, Oxygen sensors, Photoluminescence, Carbazole

Introduction

The coumarin scaffold represents a privileged molecular motif for the design of pharmacologically active molecules. In fact, compounds bearing a coumarin core have been studied as potential central nervous system drugs,[1] as anticancer,[2] anti-inflammatory,[3] and anticoagulant agents.[4] As well, a series of natural and synthetic coumarin derivatives have shown not negligible antiviral and antibacterial activity.[5] Furthermore, an essential part of the studies concerning the use of coumarin derivatives in drug discovery and technological applications focus on their electronic profiles and chemical-physical properties with particular emphasis on fluorescence.[6] It is well documented that the decoration of electron-donating groups on the coumarin benzene ring leads to highly efficient dyes.[7] For this reason, emitting coumarins have been used as metal-free luminescent sensors and probes for biological applications[8] and as site-selective bioimaging agents.[9] On the other hand, thermally stable coumarins have been proposed as useful emitters for organic light-emitting diodes[10] and as dyes for solar cells.[11] In recent years, three coumarin derivatives, endowed with high photoluminescence quantum yield (PLQY) and thermally activated delayed fluorescence (TADF) properties,[12] have been reported in the literature, respectively by Qi and co-workers in 2016 (8-(((4-(dimethylamino)phenyl)imino)methyl)-7-hydroxy-4-methyl-2H-chromen-2-one, CDPA),[13] and by Zhang in 2017, who synthesized the phenoxazine compound (9-(10H-phenoxazin-10-yl)-6H-benzo[c]chromen-6-one, PHzBCO).[14] Later in 2019, the same group reported the structurally related sky-blue emitter 9,10-dimethyldihydroacridine (MAB)[15] (Figure 1). These compounds can be described as D-π-A fluorophores in which a donor unit (D) is represented by a strongly donating heterocyclic substituent such as PHzBCO or MAB, or by a hydroxyl group as for CDPA; the acceptor moiety (A) is represented by the carbonyl-conjugated coumarin scaffold. Recently, our research group has conducted a series of photophysical studies on variously substituted coumarins, aimed at the development of new organic dyes for both OLEDs and biomedical applications.16 In particular, we evaluated the link between the PLQY and the structure of coumarin derivatives. Following these investigations, we observed that the replacement of the aryl groups with nitrogen aromatic heterocycle substituents, in particular carbazole units, amplified the optical properties of our coumarins, both in terms of PLQY and fluorescence lifetime. Coumarin-carbazoles (Figure 1) possess modest-to-large energy gaps, ∆EST, (0.29-0.57 eV) between the lowest-lying singlet (S1) and triplet (T1) excited states. A sufficiently small ∆EST allows thermally induced reverse intersystem crossing (RISC) that converts triplet excitons into singlets, generating delayed fluorescence (DF) as compared to the prompt one (PF, Figure S1).[14,17] This phenomenon and the ∆EST are also dependent on the surrounding environment. In particular, TADF dyes show sensitivity to oxygen as their triplet states are efficiently quenched by O_2.[18] A certain number of oxygen-mediated luminescence turn-off processes have been exploited for the quantification of this gas. Ratiometric oxygen sensors based on emitting organometallic complexes,[19] metal-organic frameworks (MOFs),[20] and polymers embedded with mixtures of fluorescent and phosphorescent dyes, including TADF-copolymers, have all been investigated for oxygen detection in different environments, including in vitro biological assays.[21] Herein we report the synthesis and photophysical

characterization of a series of TADF-carbazole-coumarin small molecules and the studies carried out for their use as reversible molecular oxygen sensors. For these purposes, the luminophores were incorporated into commercially available polymers, and stereolithography 3D printing of these mixtures allowed to achieve easy-to-handle thin plate sensors.
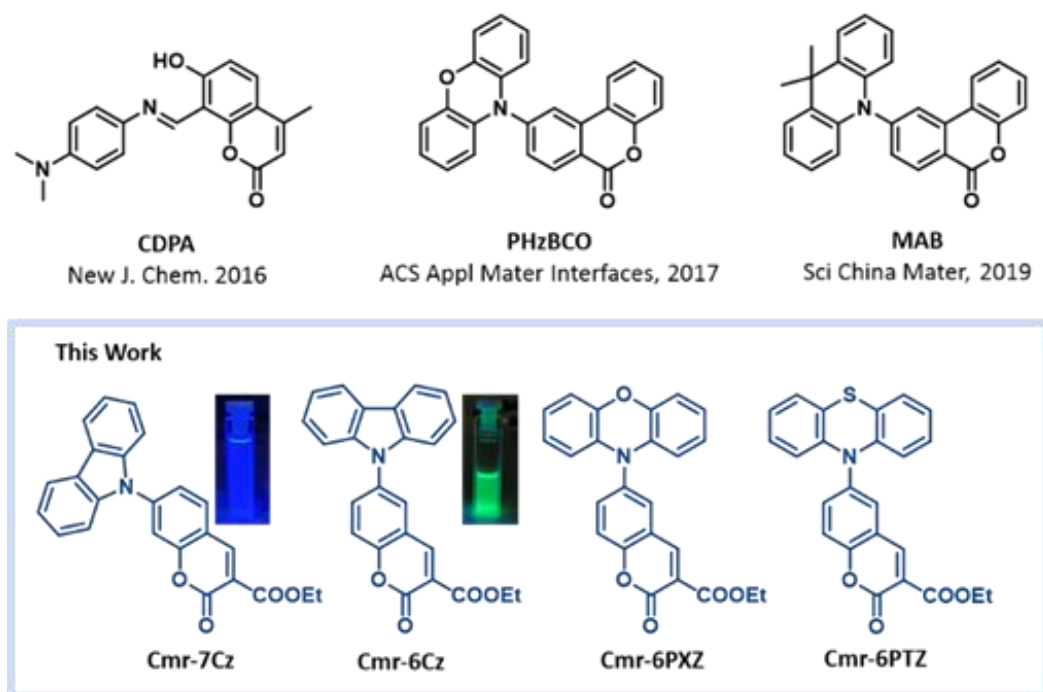
Figure 1. a) Known coumarin-based TADF molecules; b) 6- and 7-Cz-coumarins, PXZ and PTZ-coumarin scaffolds studied in this work.

Results and Discussion

Computational Insight

With the aim to explore the properties of new coumarin-based TADF derivatives, we first undertook a computational study of 3-carboxyethyl coumarin derivatives (Cmr) at the DFT level to predict their optical properties by optimizing the structures in their ground and excited states at PBE0/6-31G(d,p) level. A carbazole unit (Cz) in position 5, 6, 7 or 8 of the chromenone benzene-ring was considered together with two other stronger electron-donating substituents, phenoxazine and phenothiazine (PXZ and PTZ). The PBE0 functional was adopted to describe the electronic structure,[22] and the excited state properties being calculated within the Tamm-Dancoff approximation (Figure 2).[23]

A comparison between the lowest unoccupied molecular orbital (LUMO) of all the analyzed Cmr-Czs revealed similar energy values, indicating that the Cz is poorly electronically coupled to the same acceptor group for all the compounds; similar LUMO levels were computed also for Cmr-6PXZ and Cmr-6PTZ. Among the Cmr-Cz derivatives, positioning the carbazole unit at the 8- and 5-position (Cmr-8Cz and Cmr-5Cz) produces dyes with the smallest ΔEST (0.15 and 0.16 eV, respectively), suggesting these two compounds to potentially be TADF. By contrast,

moving the carbazole moiety to positions 6 and 7 led to compounds with ΔEST of 0.29 and 0.57 eV, respectively. However, among the evaluated structures, Cmr-7Cz presents the largest oscillator strength (*f*) for the S0-S1 transition, whilst the one with the smaller ΔEST, Cmr-8Cz, also displayed the smaller *f*; similarly, Cmr-PXZ and Cmr-PTZ possess both small ΔEST (0.02 eV), stabilized S1 states and negligible or null values of *f*. The emissive S1 state in each compound is charge-transfer in nature. Finally, we calculated the dihedral angle between the donor and the coumarin acceptor core. Depending on the nature of the donor, the designed compounds showed a calculated D-A dihedral angle between 47 and 127°, with almost perfect orthogonality observed for Cmr-6PXZ and PTZ (Table S1 in ESI).
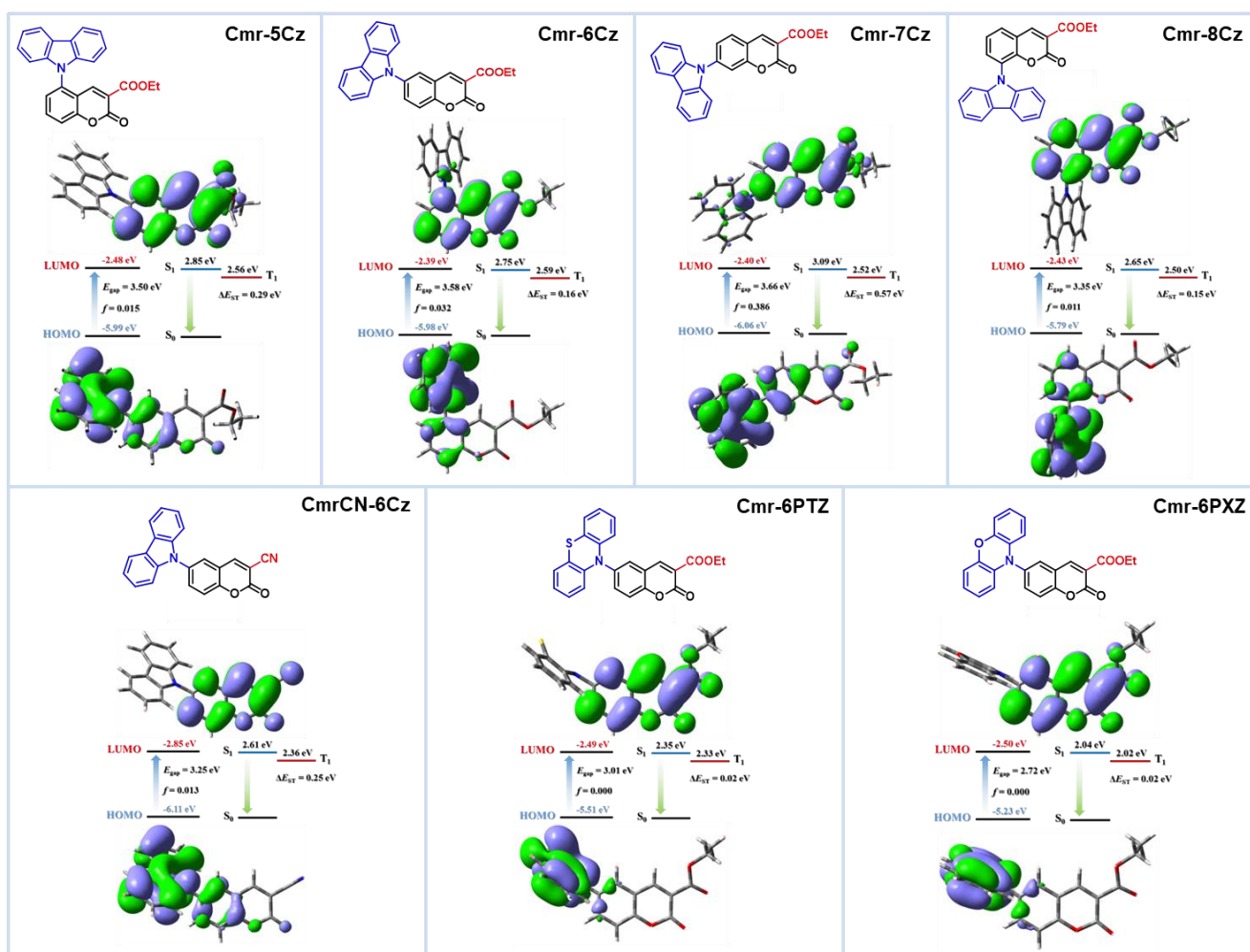

Figure 2. Computed optimized structures, molecular orbitals, and scheme of energy levels of Cmr compounds reporting band gaps (Egap), the ground state level (S0), the lowest singlet (S1) and triplet (T1) states, and oscillator strengths of S1-S0 transition.

However, we noted that the dihedral angle seems to play a less relevant role in determining the suitability as TADF molecules for this class of compounds than in other cases, since molecules with comparable dihedral angles, like Cmr-7Cz display quite different computed TADF features. The incorporation of a cyano-group onto the coumarin core (CmrCN-6Cz) was also

investigated. However, the quantum mechanical calculations for this derivative did not show a significant enhancement in the chemical and physical properties compared to the original Cmr-6Cz analogue. Instead, there was a slight reduction in the gap (down to 0.25 eV) along with a decrease in the oscillator strength (down to 0.13 eV). Finally, aiming at discussing the detected optical properties (vide infra), the conformers of Cmr-6Cz and Cmr-7Cz obtained by changing by 90° the dihedral angle between D and A were also computed (Figure S2).

Synthesis

Based on this computational study, the most promising coumarin compounds were prepared following a multigram scale two-step synthesis based on a Knoevenagel condensation reaction between the commercially available bromo-salicylaldehydes 1a-1d and diethylmalonate under mild conditions to afford the desired derivatives 2a-d in 78-90% yield. Similarly, 4-bromosalicylaldehyde was reacted with malononitrile to obtain the corresponding 6-bromocoumarin 3c in almost quantitative yields. Once recrystallized, pure bromo-coumarins were submitted to Pd(0)-catalysed Buchwald-Hartwig coupling conditions with the desired heterocyclic amines (Cz, PXZ, PTZ). Compounds Cmr-6Cz and Cmr-7Cz were obtained in 48 and 50% yield after EtOH crystallization;[24] however, this synthetic approach did not allow to isolate Cmr-5Cz and Cmr-8Cz, which were observed in trace amounts, and as inseparable mixtures from other unidentified products.
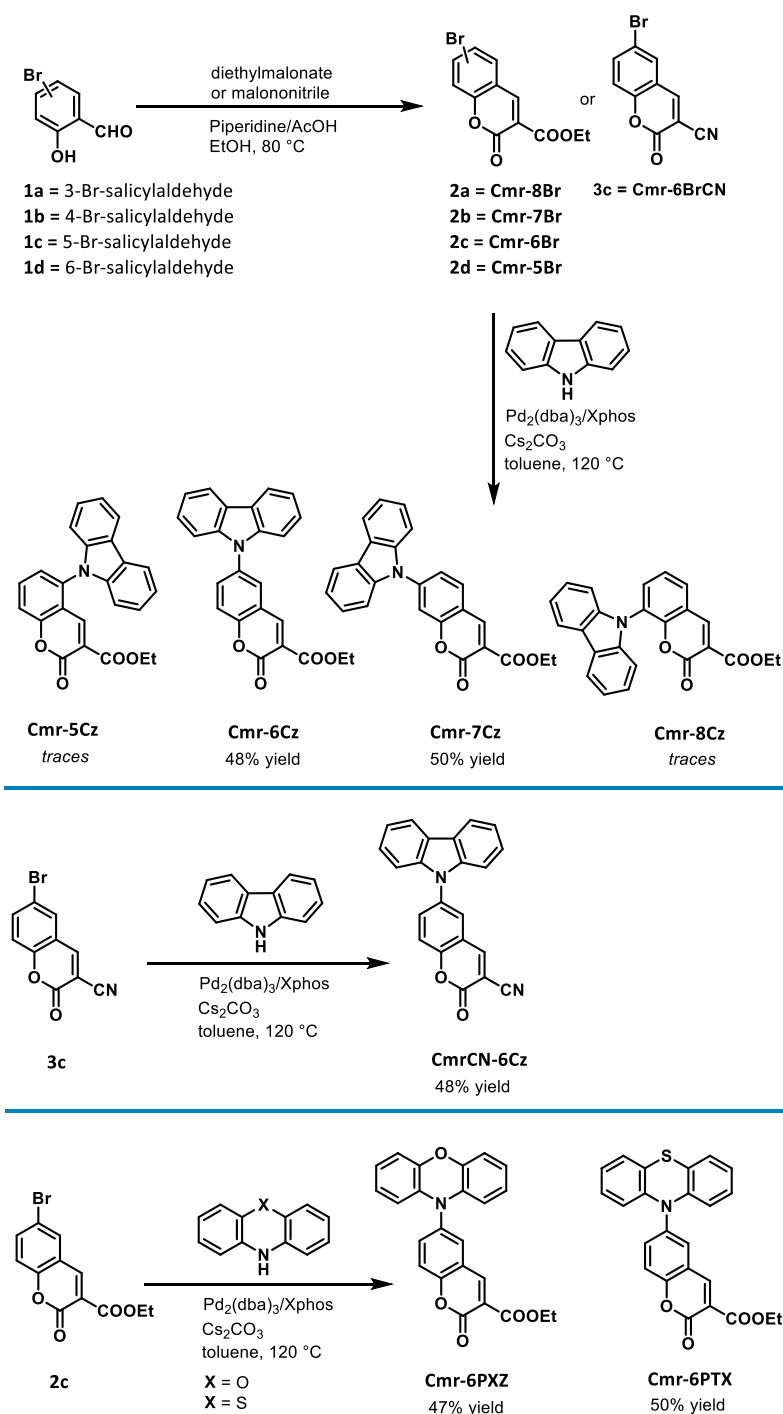
Scheme 1. Two-step synthesis of Cmr-6Cz and Cmr-7Cz, Cmr-6PXZ and Cmr-6PTX. Synthesis of CmrCN-6Cz.

Different synthetic approaches to obtain these two derivatives including reactions catalyzed by other Pd- and Cu-complexes were unsatisfactory, and studies aimed at the isolation of Cmr-5Cz and Cmr-8Cz are still ongoing. On the other hand, Cmr-PXZ and Cmr-PTZ were isolated in satisfactory yields and easily purified through crystallization. Finally, CmrCN-6Cz was isolated in 48% yield as reported in Scheme 1. To verify the computed dihedral angles θD, between the D-group and the coumarin scaffold of the Cmr-adducts25 we performed single X-ray diffraction analyses experimentally measured θD for Cmr-6Cz, Cmr-7Cz (light yellow crystals) and Cmr-

6PXZ (red crystals), Figure 3); attempts to obtain suitable crystal structures of Cmr-6PTZ (red powder) for single crystal XRD analysis were unsuccessful. The recorded values of θD = 83.73° (Cmr-6Cz), θD = 48.06° (Cmr-7Cz) and θD = 76.24° (Cmr-6PXZ) are in reasonable agreement with the computed values reported in Table S1, supporting the validity of the in-silico predictions, despite the overestimated value for the Cmr-6Cz compound (Figures S3-S5).
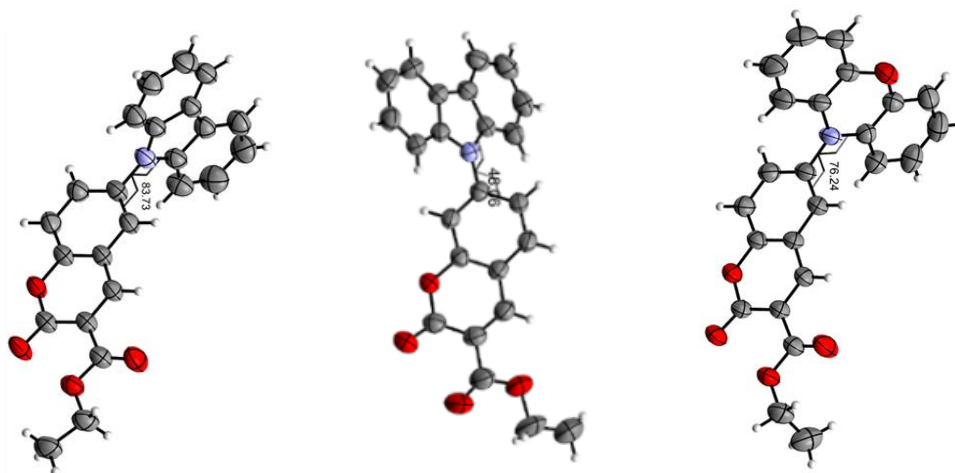
Figure 3. ORTEP representation of Cmr-6Cz (CCDC deposition number 2290080), Cmr-7Cz (CCDC deposition number 2289932) and Cmr-6PXZ (CCDC deposition number 2289931) (C = grey atoms, O = red atoms, N = blue atom, H = white atoms) and measured dihedral angles.

Photophysical Characterization of Cmr Derivatives

Toluene Cmr-derivative solutions were submitted to absorption measurements (Figure 4). Cmr-6Cz showed a broad low-energy absorption band with a maximum at about 390 nm ascribed to a CT state, followed by three higher energy narrow and intense peaks at about 340, 325, and below 300 nm linked to locally excited states. Interestingly, Cmr-7Cz displayed an inverted ratio of the intensity of these bands and a much more intense low-energy CT band. On the other hand, Cmr-6PTZ and Cmr-6PXZ have very low-intensity CT absorption bands (at about 420 and 430 nm, respectively), in line with the near-zero computed f for the CT S0-S1 transition. The study of CmrCN-6Cz was instead abandoned due to its low solubility in most of the solvents taken into consideration (Figure S6).
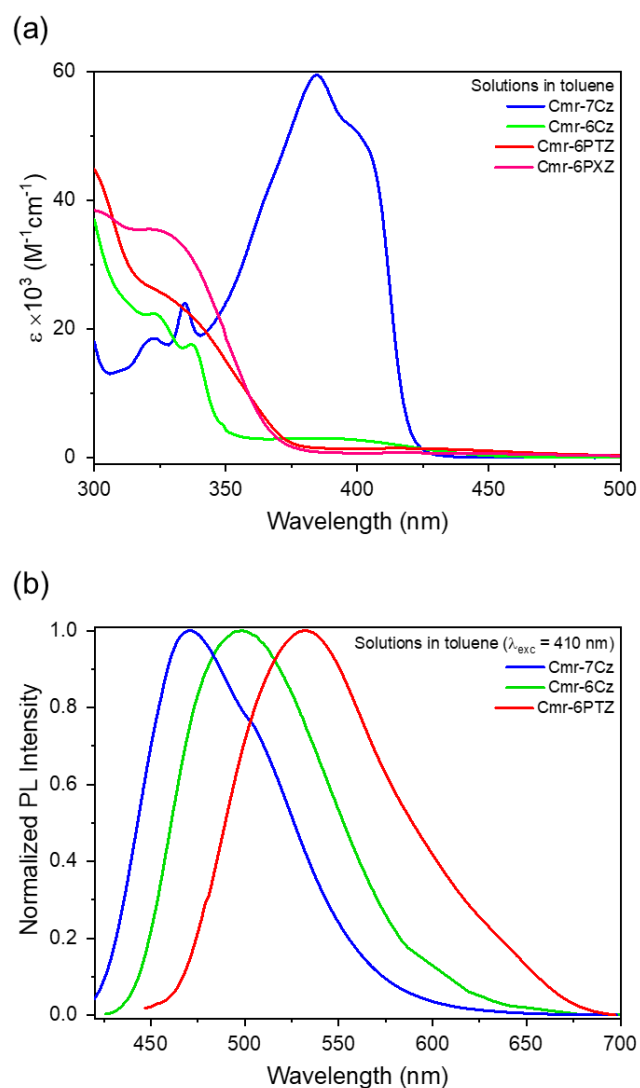
Figure 4. (a) Absorption spectra; (b) emission spectra excited at 410 nm. Cmr compounds were analyzed in toluene (10^{-5} M).

In toluene, we observed blue emission (λPL = 470 nm, with a shoulder at 505 nm) for Cmr-7Cz and green emission (λPL = 495 and 532 nm) for Cmr-6Cz and Cmr-6PXZ, respectively. No appreciable luminescence could be recorded for Cmr-6PTZ as summarized in Table 1.

Table 1. Optical features of Cmr compounds in toluene.

Samples	l_{Abs} (nm)	l_{PL} (nm)	PLQY (%)	τ_p (ns)
Cmr-6Cz	385	495	28	11.0
Cmr-7Cz	400	470	49	9.0
Cmr-6PXZ	420	532	0.5	1.5
Cmr-6PTZ	430	-	-	-

Analyses were carried out using 10^{-5} M solutions of dyes in the reported solvent. Steady-state and time-resolved emission were excited at 410 and 350 nm respectively. PLQY was estimated by means of an integration sphere exciting the samples at 350 nm.

The PLQY of all three derivatives was estimated using an integration sphere, excited at 350 nm. Cmr-6Cz and Cmr-7Cz are much brighter, with PLQY of 28 and 49%, respectively, while that of Cmr-6PXZ is 0.5%. Solvatochromic studies were carried out for Cmr-6Cz and Cmr-7Cz, using a panel of solvents including n-hexane, diethyl ether, dimethylformamide, chloroform and toluene (Figures 5a and 5b). The recorded emission spectra revealed a strong positive solvatochromic effect leading to a large red shift of the emission as the polarity of the solvent increases, paired with an overall decrease in the emission intensity and a broadening of the spectral features, as expected for compounds emitting from a CT state.[26] Finally, we carried out lifetime experiments by exciting the coumarin samples at 350 nm. In Figure 4c we report the decays for Cmr-6Cz and Cmr-7Cz in toluene, with lifetimes of 11 and 9 ns, respectively for Cmr-6PXZ a fast decay time of about 1.5 ns was estimated (Figure S7). No delayed emission was observed in these samples, likely due to the presence of fast non-radiative deactivation pathways in solution.[27] The trend of decay times in different solvents is reported in Figure S8, showing that, by increasing the polarity of the solvent, the lifetime of Cmr-7Cz increases about 4 times, from 3.5 ns in hexane to 15.0 ns in DMF. The same trend was recorded also for Cmr-6Cz. The PLQY was also evaluated for these two compounds under different environmental conditions by bubbling O2 and argon gasses into their toluene solution. PLQYs of 36 and 55% for Cmr-7Cz, and 16 and 34% for Cmr-6Cz were measured under oxygen and argon bubbling, respectively.[28] Despite the absence of any delayed emission, the presence of O_2 reduced the efficiency of the emission as compared to in-air conditions because of increased interactions between O_2 with the excited molecules in their triplet states. Finally, we performed some preliminary transient absorption spectroscopy (TAS) measurements of these two compounds in different solvents. In general, the TA spectra of both of the samples (Figure 5d) displayed broad excited state absorption (ESA) bands in the 420-500 nm and in the 600-700 nm ranges. The peak position and shape of the ESA transitions depend on the solvent polarity, as expected

for CT states. Interestingly, in the case of Cmr-7Cz in chloroform also an intense negative signal in the ΔA spectrum was detected at about 520 nm, which may be related to ground state bleaching (GSA) or stimulated emission (SE) transitions. The TA spectra as a function of the time (Figure 5e) show that both the positive ESA in the blue region and the negative GSA/SE signals reach their maximum after a few ps, as also shown by the kinetic traces in Figure 5f (the overall contour map of TA measurement is reported in Figure S9).[29] Both the solvent dependence of the ESA and the observed rise time of the signals confirm the CT character of the investigated systems and the presence of triplet localized excited (LE) and CT dark states whose solvent-dependent relative positions can largely affect the TADF efficiency.[27,29] All the experimental data coupled with the simulation results suggest that Cmr-6Cz and Cmr 7Cz samples are TADF compounds, although no delayed emission was recorded in solution, as already reported for other D-A organic systems.[27]
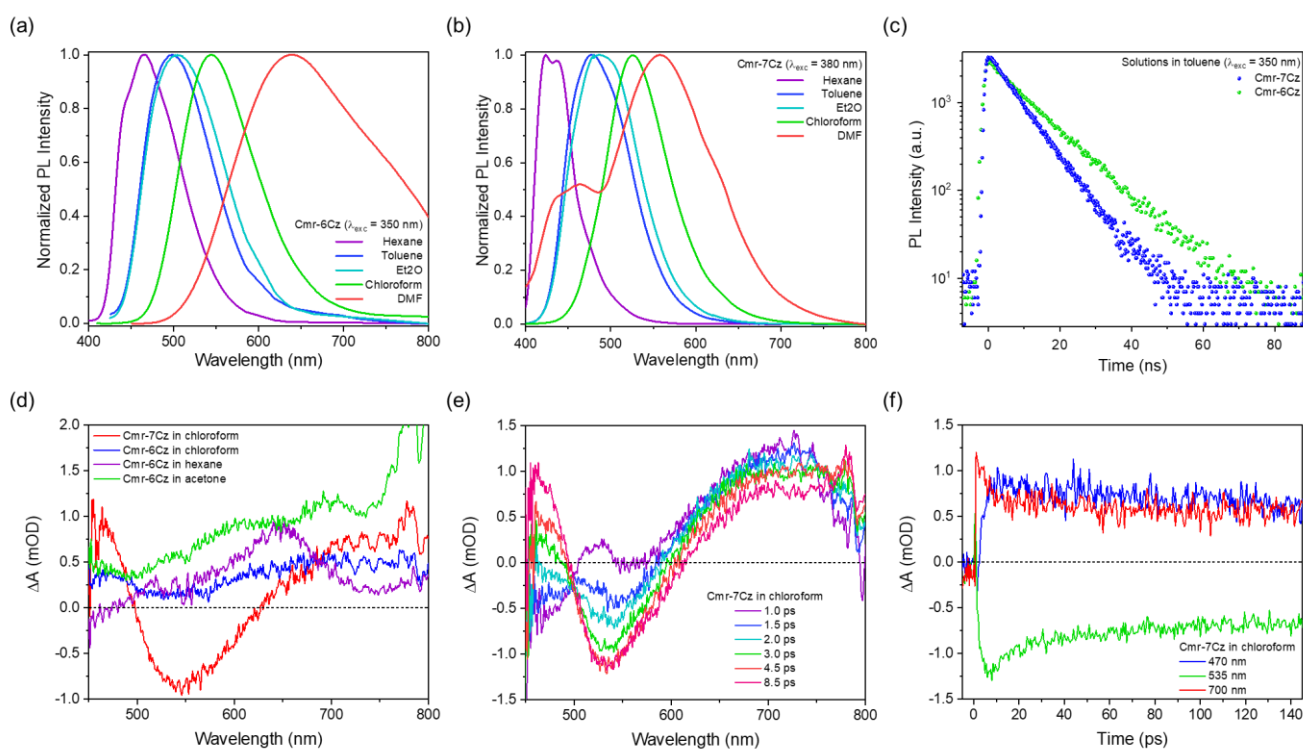

Figure 5. Cmr-6Cz (a) and Cmr-7Cz (b) emission features in different solvents; decay time plot of Cmr-6Cz and Cmr-7Cz in toluene under 350 nm excitation (c); TA spectra of Cmr-6Cz and Cmr-7Cz in different solvent pumped at 410 nm (8 ns time scale) (d); TA spectra at different probe delay of Cmr-7Cz in chloroform (150 ps time scale) (e); kinetics traces of TA signals of Cmr-7Cz in chloroform (f).

The compounds were also dispersed in PMMA films (10% w/w concentration) in an attempt to detect the delayed emission by suppressing non-radiative decay in a solid host matrix. At room temperature (Figure 6a) all Cmr-compounds emit in the green region except for Cmr-6PXZ, which emitted in the red region (Figure 6a, λPL = 495, 515, and 550 nm for -7Cz, -6Cz and -6PTZ, respectively, λPL = 610 nm for Cmr-6PXZ). Emission lifetime and PLQY measurements were

carried out at room temperature (data are summarized in Table 3). Time-resolved (TR) PL measurements under vacuum of Cmr-6Cz and -7Cz revealed the expected delayed emission. Moreover, temperature-dependent TR PL measurements confirmed that the delayed emission was thermally activated (Figure 6b-f). Measurements recorded at 77 K allowed us to observe, in the millisecond time domain, a phosphorescence emission red shifted by about 30 nm (0.13 eV) in both samples (Figure 6b and 6c).[30]
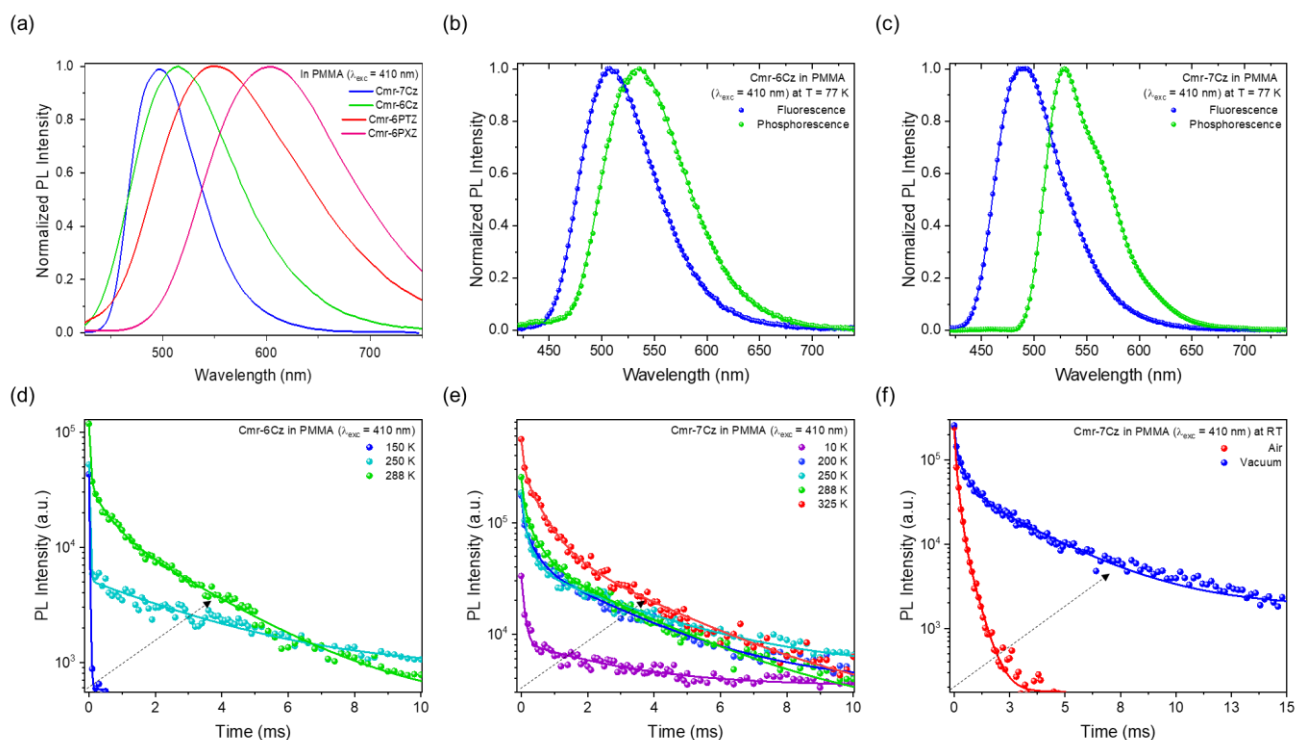

Figure 6. PL spectra of PMMA-Cmr compounds excited at 410 nm (a); fluorescence and phosphorescence spectra of the film at 77 K (b and c); decay time at different temperatures (d and e) or under different environmental conditions (f).

Finally, also in the case of the solid-state systems, we recorded the effect of oxygen on the photophysical properties of the emitters. As shown in Figure 6f, in the presence of oxygen there is a significant quenching of the delayed emission confirming the involvement of excited triplet states in the overall emission process. We observed delayed emission at room temperature, with the emission spectrum almost overlapping the prompt emission. Notably, Cmr-7Cz displayed a red shift of about 40 nm compared to Cmr-6Cz. This shift was attributed to the interaction between the guest molecule and the host matrix. Decay time plots indicated two emitting centers with similar lifetimes (Figure 7). Spectral analysis revealed two distinct contributions in both prompt and delayed fluorescence for both compounds (see Figures S10-S11 and Tables S2-S3 for more details). The dual-emitting center concept was applied to determine the relative contribution of prompt and delayed emissions.[31] Despite the similar ΔE_{ST}, we observed two different kinetics for the two samples across the time range explored, with a larger relative contribution of the delayed emission in the Cmr-6Cz sample. The analysis

showed a higher DF/PF value for Cmr-6Cz compared to Cmr-7Cz, aligning with the assessment of temperature-dependent emission features and suggesting superior TADF performance for Cmr-6Cz.

Table 2. Optical features of Cmr compounds in toluene.

Properties	Cmr-6Cz	Cmr-7Cz
λ_{PL} (nm)	508	497
PLQY (%)	11	30
S_1 (eV)	2.44	2.49
T_1 (eV)	2.32	2.35
ΔE_{ST} (eV)	0.12	0.14
τ_p (ns)	15.2	6.6
τ_d (µs)	809	395
τ_{phox} (ms)	4.5	5.9
k_p (s^{-1})	$3.44 \cdot 10^6$	$2.16 \cdot 10^7$
k_d (s^{-1})	$2.13 \cdot 10^1$	$9.05 \cdot 10^0$
k_{ISC} (s^{-1})	$3.06 \cdot 10^6$	$1.51 \cdot 10^7$
k_{RISC} (s^{-1})	$3.63 \cdot 10^1$	$1.90 \cdot 10^1$

All the measurements were recorded by exciting the samples at 410 nm at room temperature (except for T1 which was measured at 77 K). Mean decay times and transition rates are calculated according to the procedure reported in ESI. PLQY was estimated by means of integrating sphere; ΔEST was estimated by the difference between the prompt and phosphorescence emission signal. From the reported analysis, the kinetics parameters of the two emitters were extracted (Table 3), including the reverse intersystem crossing rate constant according to equation 1:

$$k_{RISC} = \frac{k_p k_d \Phi_{TADF}}{k_{ISC} \Phi_F} \qquad \text{(eq. 1)}$$

The evaluated rate constants show that in both cases the direct and reverse rates of Cmr-6Cz are slightly larger than the ones of the Cmr-7Cz, confirming the former as the most promising TADF compound.
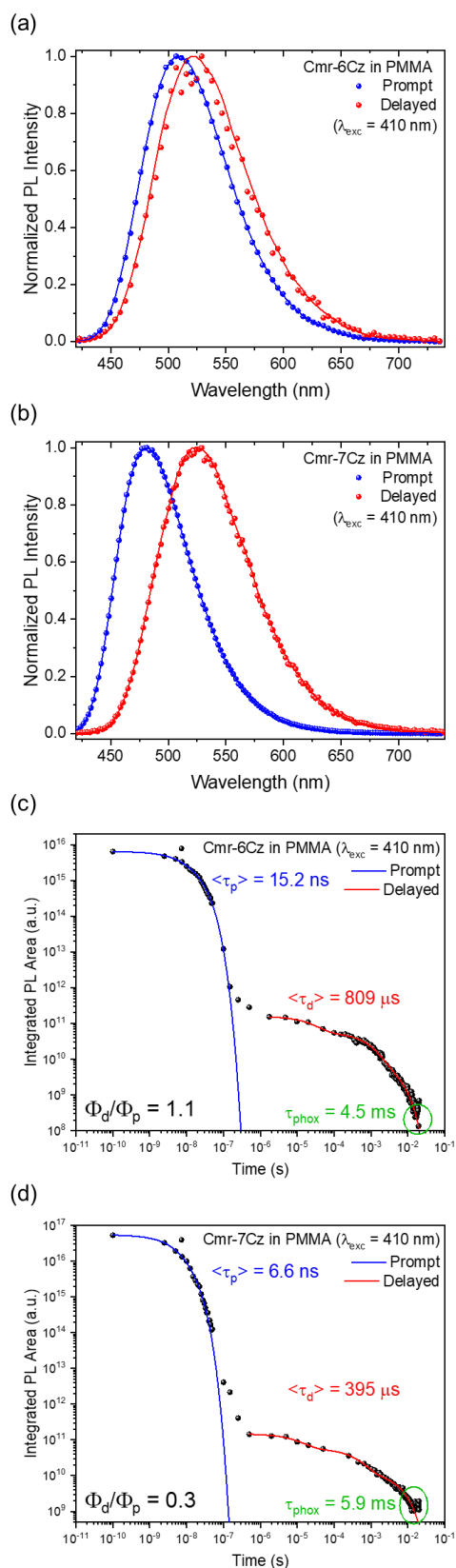
Figure 7. Prompt and delayed emission for Cmr-6Cz (a) and Cmr-7Cz (b) films; Integrated emission of Cmr-6Cz (c) and Cmr-7Cz (d) films over different time range with fit results, mean lifetime of prompt, delayed and phosphorescence emissions, and estimated ratio between delayed and prompt contributions. Samples were excited at 410 nm.

Electrochemical properties of Cmr-6Cz and Cmr-7Cz were also performed (Figure S12). Cmr-6Cz shows a reduction peak at -1.22V (vs SCE), whereas Cmr-7Cz presents a cathodic wave at -1.24 V. From the CV curves the reduction and oxidation potentials are retrieved, at -1.22V/-1.17V and -1.24V/-1.17V for the two compounds respectively. Consequently, the energy band gap of 2.39 eV (518 nm) and 3.44 eV (518 nm) are estimated, in reasonable agreement with our UV/VIS measurements. [28,31]

Oxygen sensing studies

Cmr-6Cz and Cmr-7Cz PMMA films were finally investigated as solid-state oxygen sensors. To pursue in these investigations, the polymeric samples were placed first under an inert nitrogen atmosphere and the partial pressure of oxygen was gradually increased: as the oxygen pressure increased, the PL intensity continuously decreased (Figure 8a and 8c). The emission intensity ratio in N_2 vs the emission intensity in O_2 was evaluated from the spectra. The estimated emission intensity ratio was 1.51 and 1.47 for Cmr-6Cz and Cmr-7Cz, respectively. The dependence of the integrated emission intensity on the O_2 concentration was then analysed using the Stern-Volmer equation (eq. 2), describing the non-linear curves reported in Figure 8b and 8d, for the Cmr-6Cz and -7Cz samples respectively.[35] In eq. 2 $I0$ and I represent the integrated emission intensities under nitrogen and at different oxygen concentrations; fc is the fractional contribution of one of the two different centres participating in the bi-molecular process causing the emission quenching; K^1_{SV} and K^2_{SV} are the Stern-Volmer constants of the two sites and pO_2 is the relative pressure of O_2.

$$\frac{I_0}{I} = \frac{1}{\frac{fc}{1+K^1_{SV}\, pO_2} + \frac{1-fc}{1+K^2_{SV}\, pO_2}} \qquad \text{(eq. 2)}$$

The nonlinear Stern-Volmer plots suggest that there are two different quenching processes: the first one is very fast and reactive even at low oxygen pressure and accounts for about 90% of the reactive sites (fc is equal to 91 and 86% for Cmr-6Cz and Cmr-7Cz, respectively); the second one is relatively slow and allows some residual fluorescence, which is not quenched by oxygen. The existence of domains less permeable to oxygen in our solid-state samples may be responsible for the non-linearity of the reported curves.[36] Despite the overall low sensitivity to oxygen,[34,35] the high precision fitting by eq. (2) for both compounds (R values of 0.99 and 0.98 for Cmr-6Cz and Cmr-7Cz, respectively) can be exploited to precisely evaluate the oxygen concentration by measuring the ratiometric photophysical properties of the film samples. The observation of residual emission for atmospheric oxygen pressure agrees with the results of the PL decay measurements for these compounds in PMMA films under vacuum or under air (Figure 6f), confirming that these systems are characterized by delayed fluorescence, even in the presence of O_2.[35]
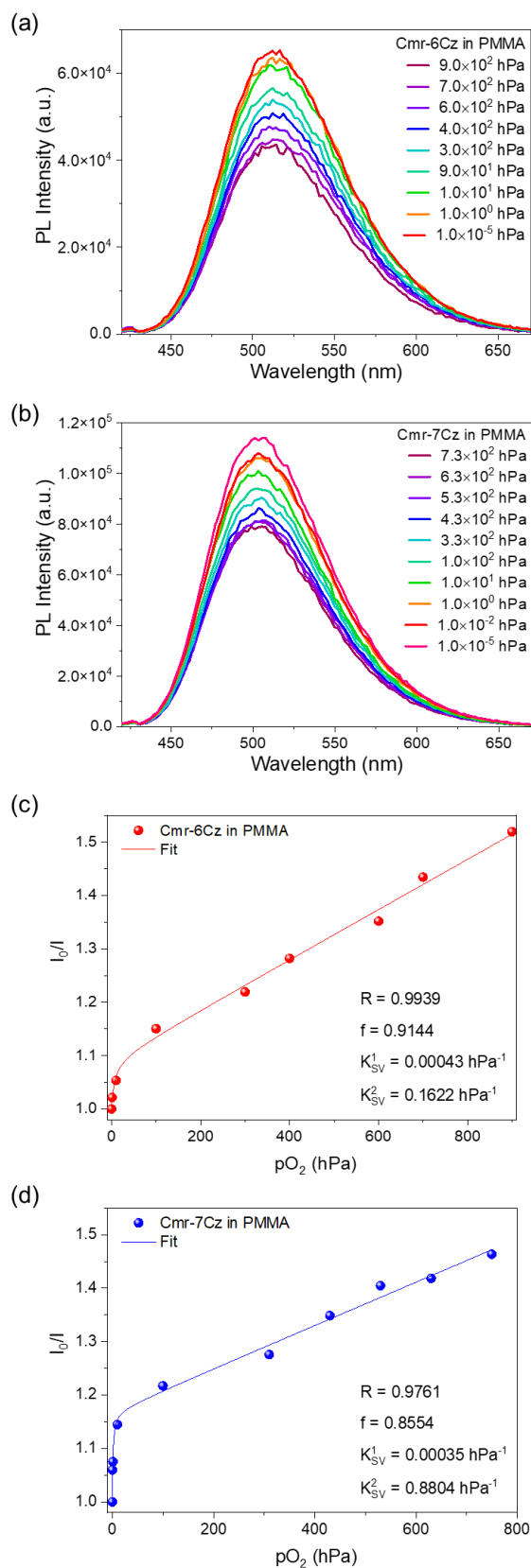
Figure 8. Cmr-6Cz (a) and Cmr-7Cz (c) PL spectra with different partial pressure of O₂ within the experimental chamber and corresponding Stern-Volmer plot of Cmr-6Cz (b) and Cmr-7Cz (d). Samples were excited at 410 nm.

To assess the possible application of the two PMMA systems as O_2 sensors we measured repeatedly the emission spectrum in air and under vacuum conditions. Once the oxygen was removed the delayed emission increased in both samples by 6 times, the on/off switching being reproducible several times within the uncertainty level of the experiment. On the contrary, the prompt emission of both emitters was insensitive to the environment conditions, being constant during the oxygen on/off measurements. Clearly, when integrating the overall signal on a millisecond scale, Cmr-6Cz is more efficient for detecting the presence of oxygen because of the relatively higher contribution of the delayed emission with respect to the prompt one (Figure 9). Subsequent evaluation of these emitters as O_2 sensors in HDDA and Tegorad matrices was not possible due to the almost total suppression of the delayed emission in both cases, showing that the selection of the matrix is crucial to achieve a viable O_2 sensor (Figure S12). Although various ratiometric TADF-systems are known for the determination of O_2,[37] our prototype Cmr-7Cz-PMMA (K^1_{sv} = 0.00035hPa-1; K^2_{sv} = 0.8804hPa-1) fits well among oxygen sensors characterized by high sensitivity, reproducibility, reversibility and low cost (figure 8c and 8d). Indeed, various sensors already reported in the literature are based on the use of organometallic complexes including Zn[38] or other critical transition metals like iridium.[19] On the other hand, photoluminescent TADF copolymers seems to be limited due to their synthetic complexity.[20] In this scenario, a device obtained from small, easily preparable organic molecules embedded in commercially available and inexpensive polymeric resins, is certainly advantageous and prone of further applicability in sensing technologies.
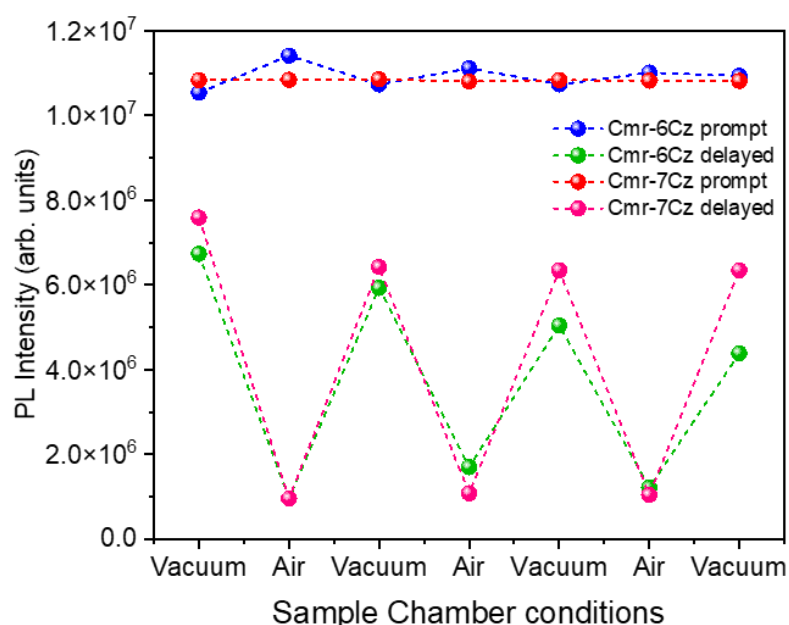
Figure 9. Variation of integrated PL intensity recorded for the prompt and delay fluorescence of Cmr-6Cz and Cmr-7Cz under different sample chamber conditions (vacuum and air). Samples were excited at 410 nm.

Biocompatibility of Cmr derivatives

With the aim of assessing their potential as dyes for biomedical applications, we conducted a series of biological tests on both normal and cancer cell lines using the MTT assay, with camptothecin as a positive control. Thyroid cells, SK-MES-1, Vero-76, CCRF-CEM, and WIL-2NS were separately treated with varying doses of both Cmr-6Cz and Cmr-7Cz (ranging from 10 μM to 100 μM). After a 24-hour incubation period, 3-(4,5-dimethylthiazol-2-yl)-2,5-diphenyltetrazolium bromide (MTT) was added, and the optical density was measured at 550/690 nm using a microplate reader. The cell growth/viability at each concentration of coumarin was expressed as a percentage of untreated controls. Concentrations resulting in 50% inhibition (CC_{50}) were determined through linear regression analysis, with all tests conducted in triplicate. As indicated in Table 3, both coumarins demonstrated no cytotoxicity against any of the cell lines tested (CC50 >100 μM).[39]

Table 3. In vitro cytotoxic effects of **Cmr-6Cz** and **Cmr-7Cz** and reference compound Camptothecin against different cancer and normal cell lines.

| CC_{50} (μM)[a]	Cmr-6Cz	Cmr-7Cz	Camptothecin
SK-MES-1	>100	>100	0.006 ± 0.003
Vero-76	>100	>100	-
CCRF-CEM	>100	>100	-
WIL-2NS	>100	>100	-
TPC-1	>100	>100	0.01 ± 0.02
Nthy-ori-3-1	>100	>100	0.01 ± 0.02

CC_{50}: compound concentration required to inhibit cell proliferation by 50%. Data are expressed as the mean ± SD from the dose-response curves of at least three independent experiments.

Furthermore, Nthy-ori-3-1 cells were incubated with 1 μM of Cmr-6Cz and analysed using a fluorescence microscope. In vitro cellular imaging was conducted utilizing a digital image analysis system with blue and orange filters. Figure 10 illustrates the fluorescence emitted by Cmr-6Cz in the treated cells (b). DAPI staining of the nucleus (a) revealed that Cmr-6Cz predominantly distributed in the cytoplasmic region, with minimal fluorescence observed in the nucleus. The merging of emission from Cmr-6Cz and DAPI confirmed the cytoplasmic targeting of this coumarin (c). In contrast, control cells without treatment with the coumarin derivative exhibited no fluorescence.
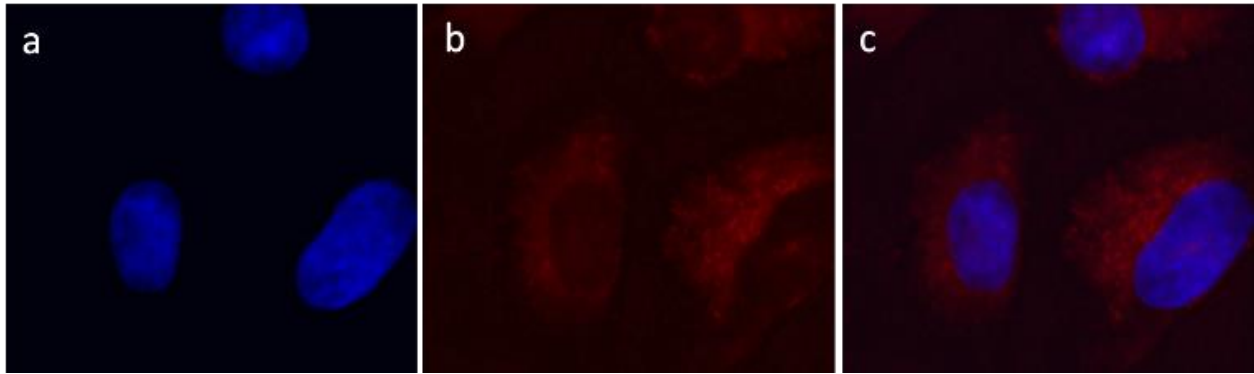
Figure 10. Cellular imaging of Nthy-ori3–1 cells treated with Cmr-6Cz coumarin (1µM). a) representative nuclei in the blue field (DAPI); b) in the orange field (Cmr-6Cz); C) merge (Cmr-6Cz /DAPI). (Exc. 470-495 nm and 530-550 nm).

H2DCF-DA method was employed to assess the effect of ROS production induced by Cmr-6Cz and Cmr-7Cz on normal thyroid cells. As illustrated in Figure 11a, coumarins tested at 10 µM significantly decreased the basal intracellular ROS production in a time-dependent manner ($p<0.05$). The generation of ROS induced by H_2O_2 was notably increased when compared to untreated cells ($p<0.05$). Conversely, Cmr-derivatives effectively reduced intracellular ROS production in H_2O_2-treated cells in a time-dependent manner ($p<0.01$). Additionally, cells treated with different concentrations of Cmr-6Cz or Cmr-7Cz (10 µM, 20 µM, 30 µM, and 40 µM) did not exhibit a dose-dependent ROS-scavenging effect (Figure 11b and c).
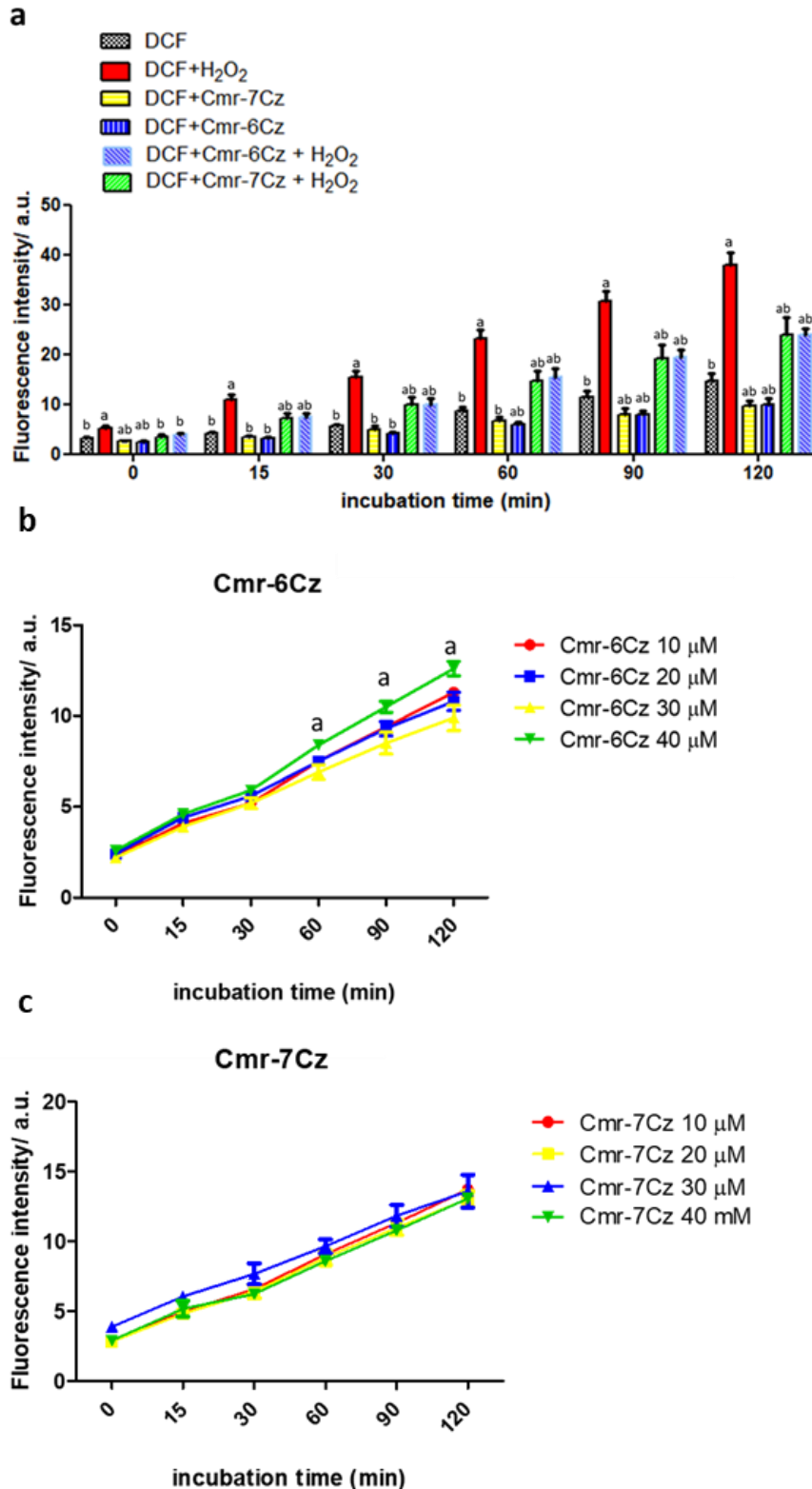
Figure 11. ROS level, visualized as H2-DCF-DA fluorescence and expressed as arbitrary units (a.u), in Nthy-ori3-1 cells after treatment with Cmr-7Cz and Cmr-6Cz. a) Cmr-7Cz and Cmr-6Cz treatment reduced ROS generation in the Nthy-ori3-1 cells at different time points (0,15,30,60,90, 120 minutes) after incubation with or without H_2O_2; b) and c) ROS production by different concentrations of Cmr-6Cz and Cmr-7Cz. Values not sharing a superscript letter are significantly different ($p \leq 0.05$). These findings suggest that both coumarins not only

possess radical scavenging activity but also demonstrate efficacy as potent inhibitors against hydrogen peroxide-induced cellular oxidative stress.

Conclusion

In this study, we have demonstrated how the insertion of carbazole heterocyclic derivatives on the benzene ring of coumarin scaffolds allows access to new biocompatible organic dyes characterized by good photoluminescence quantum yields and TADF properties. The prediction and design of these compounds were guided by quantum chemical calculations that highlighted the potential value of Cmr-Cz adducts as TADF emitters. These results were corroborated by experimental findings, which validated these predictions. TADF properties of carbazolyl-coumarins were explored in solution and in the solid state by embedding the dyes in PMMA. A Cmr-PMMA-based sensor for O_2 detection was also produced, demonstrating the utility of these compounds. In in vitro cultures, these compounds have demonstrated cytoplasmic distribution and a notable action as radical scavengers, protecting cells from oxidative stress. Currently, new studies aimed at developing intracellular fluorescent sensors and utilizing these derivatives as fluorescent probes with potential applications in bioimaging are underway.

Authors contribution

The manuscript was written through contributions of all authors. All authors have given approval to the final version of the manuscript. A. C. and S.P. performed the synthesis and the NMR characterization of all the compounds cited in this article. C.O., R.C., P.C.R, L.P. performed the photophysical characterization of Cmr-compounds. F.S. designed the project, analysed the data, and supervised the research together with E. Z.-C. and C.M.C.

Acknowledgements

References and Notes

[1]   a) K. Skalicka-Woźniak, I. Erdogan Orhan, G. A. Cordell, S. M. Nabavi, B. Budzyńska, Pharmacol. Res. 2016, 103, 188-203; b) J. Kowalczyk, B. Budzyńska, Ł. Kurach, D. Pellegata, N. S. El Sayed, J. Gertsch, K. Skalicka-Woźniak, Sci. Rep. 2022, 22, 1-13.

[2]   M. Koley, J. Han, V. A. Soloshonok, S. Mojumder, R. Javahershenas, A. Makarem, RSC Med. Chem. 2024, https://doi.org/10.1039/D3MD00511A.

[3]   J. Grovera, S. M. Jachak, RSC Adv. 2015, 5, 38892-38905.

[4]   R. M.F. van Schie, T. I. Verhoef, A. de Boer, F. J. M. van der Meer, W. K. Redekop, T. Schalekamp, A.-H. Maitland-van der Zee, Pharmacogenetics of Coumarin Anticoagulant Therapy, Ed. Springler, 2015, 9, 307-328.

[5]   a) U. R. Abdelmohsen, A. Albohyc, B. S. Abdulrazikc, S. A. L. Bayoumid, L. G. Malakd, I. S. A. Khallafd, G. Bringmann, S. F. Farag, RSC Adv. 2021, 11, 16970-16979; b) L R. Singh, S. R. Avula, S. Raj, A. Srivastava, G. R. Palnati, C. K. M. Tripathi, M. Pasupuleti, K. V. Sashidhara, J. Antibiot. 2017, 70, 954-961.

[6]   D. Cao, Z. Liu, P. Verwilst, S. Koo, P. Jangjili, J. S. Kim, W. Lin, Chem. Rev., 2019, 119, 10403–10519.

[7]   Z.-S. Wang, Y. Cui, Y. Dan-oh, C. Kasada, A. Shinpo, K. Hara, J. Phys. Chem. C, 2008, 112, 17011-17017.

[8]   X.-Y. Sun, T. Liu, J. Sun, X.-J. Wang, RSC Adv. 2020, 10, 10826-10847.

[9]   Y. Cao, X. Liu, J. Zhang, Z. Liu, Y. Fu, D. Zhang, M. Zheng, H. Zhang, M.-H. Xu, ACS Chem. Neurosci. 2023, 14, 829-838.

[10]   A. Genco, A. Ridolfo, S. Savasta, S. Patanè, G. Gigli, M. Mazzeo, Adv. Opt. Mater. 2018, 6, 1800364-1800370.

[11]   R. Pradhan, H. Dahiya, B. P. Bag, M. L. Keshtov, R. Singhal, G. D. Sharma, A. Mishra, J. Mater. Chem. A, 2021, 9, 1563-1573.

[12]   Prentice, J. Morrison, A. D. Smith and E. Zysman-Colman, Chem. Eur. J. DOI:10.1002/chem.202202998.

[13]   L. Q. Yan, Z. N. Kong, Y. Xia and Z. J. Qi, New J. Chem., 2016, 40, 7061-7067.

[14]   J.-X. Chen, W. Liu, C.-J. Zheng, K. Wang, K. Liang, Y.-Z. Shi, X.-M. Ou and X.-H. Zhang, ACS Appl Mater Interfaces, 2017, 9, 8848–8854.

[15]   K. Ke, J.-X. Chen, M. Zhang, K. Wang, Y.-Z. Shi, H. Lin, C.-J. Zheng, S.-L. Tao, X.-H. Zhang, Sci China Mater, 2019, 62, 719–728.

[16]   a) A. Luridiana, G. Pretta, D. Chiriu, C. M. Carbonaro, R. Corpino, F. Secci, A. Frongia, L. Stagi, P. C. Ricci, RSC Adv. 2016, 6, 22111-22120; b) A. Cocco, P. Caria, G. Sanna, L. Stagi, E. Cadoni, R. Corpino, P. C. Ricci, C. M. Carbonaro, F. Secci, ACS Omega, 2021, 6, 33708-33716.

[17]   S. Paredis, T. Cardeynaels, S. Brebels, J. Deckers, S. Kuila, A. Lathouwers, M. Van Landeghem, K. Vandewal, Danos, A. P. Monkman, B. Champagne, W. Maes, Phys. Chem. Chem. Phys. 2023, 25, 29842-29849.

[18]   a) Y. Long, M. Mamada, C. Li, P. Lays dos Santos, M. Colella, A. Danos, C. Adachi, A. Monkman, J. Phys. Chem. Lett. 2020, 11, 3305-3312; b) M. Micheva, S. Baluschev, K. Landfester, J. Mater. Chem. C, 2022, 10, 4533-4545.

[19]   K. S. Choung , K. Marroquin, T. S. Teets, Chem. Sci. 2019, 10, 5124-5132.

[20]   X.-Y. Dong, Y. Si, J.-S. Yang, C. Zhang, Z. Han, P. Luo, Z.-Y. Wang, S.-Q. Zang, T. C. W. Mak, Nat. Commun. 2020, 11, 3678-3687.

[21]   C. M. Tonge, N. R. Paisley, A. M. Polgar, K. Lix, W. R. Algar, Z. M. Hudson, ACS Appl. Mater. Interfaces, 2020, 12, 6525-6535.

[22]   a) F. Gygi, A. Baldereschi, Phys. Rev. Lett. 1989, 62, 2160-2163; b) J. Ang, S. Falletta, A. Pasquarello, npj Comput Mater. 2023, 9, 108-117.

[23]   a) C. M. Isborn, N. Luehr, I. S. Ufimtsev, T. J. Martínez, J. Chem. Theory Comput. 2011, 7, 1814-1823; b) A.-S. Hehn, B. Sertcan, F. Belleflamme, S. K. Chulkov, M. B. Watkins, J. Hutter, J. Chem. Theory Comput. 2022, 18, 4186-4202.

[24]   A synthetic approach for Cmr-7CZ was previously reported. However, no photophysical investigations were reported to disclose its TADF properties. R. Su, Y. Zhao, S. Liu, P. Li, J. Ma, D. Zhang, M. Han and T. Yu, New J. Chem. 2022, 46, 6793-6803.

[25]   Single Crystal X-Ray Diffraction data for Cmr-6CZ (CCDC deposition number 2290080), Cmr-7CZ (CCDC deposition number 2289932) and Cmr-6PXZ (CCDC deposition number 2289931).

[26]   K. Stavrou, L. G. Franca and A. P. Monkman, ACS Appl Electron Mater, 2020, 2, 2868-2881.

[27]   X. Zhang, X. Zhao, K. Ye, J. Zhao, Chem. Eur. J. 2023, 29, e202203737, DOI:10.1002/chem.202203737.

[28]   G. Xie, X. Li, D. Chen, Z. Wang, X. Cai, D. Chen, Y. Li, K. Liu, Y. Cao and S.-J. Su, Adv. Mat. 2016, 28, 181-187.

[29]   Q. Zhang, Y. Liu, Z. Jiang, T. Guan, Y. Yang, C. Qin and Y. Liu, J Lumin, 2023, 253, 119459.

[30]   K. Albrecht, K. Matsuoka, K. Fujita and K. Yamamoto, Angew. Chem. Int. Ed. 2015, 54, 5677-5682.

[31]   K. Szychta, B. Koszarna, M. Banasiewicz, A. Sobolewski, O. O'Mari, J. A. Clark, V. I. Vullev, C. A. Barboza and D. T. Gryko, J. Am. Chem. Soc. 2023, 3, 1918-1930.

[32]   F. B. Dias, T. J. Penfold and A. P. Monkman, Methods Appl Fluoresc. 2017, 5, 012001.

[33]   F. B. Dias, J. Santos, D. R. Graves, P. Data, R. S. Nobuyasu, M. A. Fox, A. S. Batsanov, T. Palmeira, M. N. Berberan-Santos, M. R. Bryce and A. P. Monkman, Adv. Sci. 2016, 3, 1600080.

[34]   U. Tsiko, O. Bezvikonnyi, D. Volyniuk, B. F. Minaev, J. Keruckas, M. Cekaviciute, E. Jatautiene, V. Andruleviciene, A. Dabuliene and J. V. Grazulevicius, Dyes Pigm. 2022, 197, 109952.

[35]   M. Mahmoudi, J. Keruckas, K. Leitonas, S. Kutsiy, D. Volyniuk and J. V. Gražulevičius, J. Mater. Res. Technol. 2021, 10, 711-721.

[36]   A. Steinegger, I. Klimant and S. M. Borisov, Adv Opt Mater. 2017, 5, 1700372.

[37]   M. Mondal, I. Giri, R. Patra, M. Das, R. K. Vijayaraghavan, Chem. Mater. 2023, 35, 6527–6537.

[38]   S. E. Zieger, A. Steinegger, I. Klimant, S. M. Borisov, ACS Sens. 2020, 5, 4, 1020.

[39]   P. Caria, T. Dettori, D. V. Frau, D. Lichtenzstejn, F. Pani, R. Vanni, S. Mai, J. Cell. Physiol. 2019, 234, 5175-5185.